Research Square

Preprints are preliminary reports that have not undergone peer review.
They should not be considered conclusive, used to inform clinical practice,
or referenced by the media as validated information.

A full-flow microfluidic platform for synthesis, purification and concentrating of lipid nanoparticles (LNPs)

Jian Tao
Tianjin University
Junxiang Zhao
Asymchem Life Science (Tianjin) Co., Ltd.
Yuanyuan Liu
Asymchem Life Science (Tianjin) Co., Ltd.
Liang Hu
huliang11427@asymchem.com.cn
Asymchem Life Science (Tianjin) Co., Ltd.
Hongru Zhou
Asymchem Life Science (Tianjin) Co., Ltd.
Bohui Wang
Asymchem Life Science (Tianjin) Co., Ltd.
Yong Kang
Tianjin University

Research Article

Keywords: Lipid nanoparticles (LNPs), Microfluidic, Full-flow process, Mixing, Encapsulation efficiency

Posted Date: August 14th, 2026

DOI: https://doi.org/10.21203/rs.3.rs-10570513/v1

License: This work is licensed under a Creative Commons Attribution 4.0 International License.
Read Full License

Additional Declarations: No competing interests reported.

A full-flow microfluidic platform for synthesis, purification and concentrating of lipid nanoparticles (LNPs)

Jian Tao[a,b,*], Junxiang Zhao[b], Yuanyuan Liu[b], Liang Hu[b,*], Hongru Zhou[b], Bohui Wang[b], Yong Kang[a]

a. School of Chemical Engineering and Technology, Tianjin University, Tianjin 300350, P.R. China;

b. Asymchem Life Science (Tianjin) Co., Ltd., Tianjin 300457, P.R. China

Corresponding author 1: Jian Tao, E-mail: taojian@asymchem.com.cn

Corresponding author 2: Liang Hu, E-mail: huliang11427@asymchem.com.cn

Abstract: Lipid nanoparticles (LNPs) have been widely researched as a promising delivery approach for nucleic acid therapeutics. However, the preparation of LNPs typically requires multiple manual steps conducted by experienced researchers, which is time-consuming, low-yield and of great inter-batch variability. To improve the efficiency and quality consistency, a full-flow microfluidic platform was designed, composed of a mixing module, a dilution module and a post-processing module. The platform excludes materials transfer and additional post processing steps. The end-to-end synthesis, purification and concentrating of LNPs can be completed in less than 15 min. Using on the microfluidic system, LNPs with a wide size range can be prepared at different flow conditions, revealing a negative correlation between LNPs' size and total flow rate. Furthermore, the preparations of patisiran LNPs were conducted using different lipids and siRNA concentrations. The size distributions agreed well with Gaussian functions with an average of about 100nm. Under the standard condition, the encapsulation efficiency was increased from 85.7% to 98.7% using the single-Pass Tangential Flow Filtration (SPTFF). The microfluidic process integration developed in this work was demonstrated with high efficiency and high yield, preparing LNPs for direct use in cell experiments and drug formulations. Overall, The integrated full-flow solution contributes to further R&D of LNPs and green manufacturing of high-end pharmaceutical preparations.

Keywords: Lipid nanoparticles (LNPs); Microfluidic; Full-flow process; Mixing; Encapsulation efficiency;

1. Introduction

Generally, lipid nanoparticles (LNP) refers to colloidal carriers with size less than 100 nm, which consists of ionizable cationic lipid, helper lipid, cholesterol, and PEGylated lipid. The nucleic acids

are encapsulated inside the LNPs [1-3]. Recently, LNPs have been widely studied as the delivery approach for nucleic acids [4-6]. Many nucleic acids, such as the message RNA (mRNA), small interfering RNA (siRNA), antisense oligonucleotide (ASO) and clustered interspaced short palindromic repeats (CRISPR) can be encapsulated in LNPs and delivered into the cells [5,7-10]. Several types of LNPs show great potential in exogenous gene expression, gene regulation and gene editing, which is promising in vivo genomic medicines. Due to the great commercial success in mRNA SARS-CoV-2 vaccines and Onpattro® [11-13], more new LNP-based drugs are being researched in the laboratory or in the clinical verification of cancer immunotherapy, infectious diseases and genetic orphan diseases [14-17]. Additionally, some LNPs developed with new lipids or through size precision control exhibit some interesting characteristics like organ selective delivery or blood-brain barrier penetration [18-21].

LNPs are formed through self-assembly driven by electrostatic and hydrophobic interactions [22]. During the preparation of LNPs, lipids and RNAs are rapidly mixed in an acidic solution. The cationic lipid carries a positive charge and can bind to RNAs via electrostatic interaction [23]. However, excess ionizable cationic lipids hinder the formation of intact LNPs due to electrostatic repulsion caused by surplus positive charges. Subsequently, the pH of the mixed solution is changed to neutral, decreasing positive charges and electronic repulsion [24-26]. After purification and concentration, the LNPs are completely prepared for cell experiments.

However, the development of LNP-based drugs is significantly limited by the technical complexities of synthesis and purification of LNPs. Impingement jets mixer (IJM) made by Kanuer or laboratory self-made microfluidic devices are generally used for the preparation of LNPs [27-29]. The synthesized LNPs are subsequently transferred to remove the impurities by dialysis or ultrafiltration [30,31]. The material transfer and additional post processing cause great risks in contaminations of LNPs. The traditional methods of synthesis and purification of LNPs are time-consuming, low-yield, poor batch-consistency and more experience required. Therefore, a user-friendly and contamination-free equipment is urgently required for the synthesis and post processing of expected LNPs.

Microfluidic chips can precisely manipulate extreme small volume of sample to achieve a wide range of chemical and biological process [32,33]. A well designed microfluidic chip can easily provide the rapid mixing function in milliseconds which is required in LNP synthesis and reduce the impingement to protect RNAs. Some other functions, like rapid dilution, online purification and

concentration which is required in LNP synthesis can also be achieved by microfluidic devices. The "continuous flow" nature of microfluidic device, which means the liquid was simplify flow in, being processed and flow out from the microfluidic chips, makes microfluidic devices easily integrate to a total continuous flow platform.

In the present study, a full-flow microfluidic method was advanced for the synthesis, purification and concentrating of LNPs. The end-to-end process could be rapidly completed within 15min. The encapsulation was experimentally demonstrated with patisiran LNPs. Without material transfer and additional post processing, the LNP-based products have little possibility of contamination and can be directly used in cell experiments, as shown in Figure 1. LNPs with different sizes can be prepared through changing flow conditions. The full-flow microfluidic solution could contribute to the R&D of more LNP-based drugs and green manufacturing.

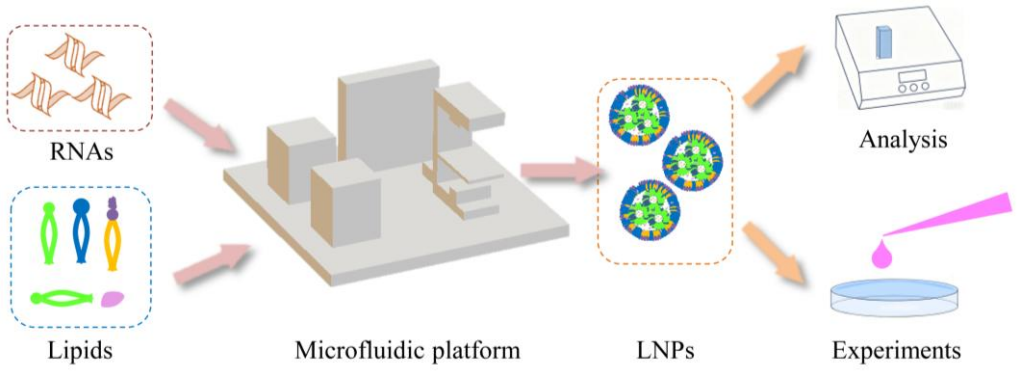

Figure 1 End-to-end solution of LNPs synthesis

2. Experimental platform

The microfluidic platform consisted of mixing module, dilution module and post-processing module, as shown in Figure 2. The microfluidic chip in mixing module could achieve rapid mixing of water and ethanol in several milliseconds. Simultaneously, lipids dissolved in the ethanol and RNA dissolved in the water were self-assembled to form LNP precursor, driven by electrical and hydrophobic interactions. Then the mixed solution flowed into the dilution module in several seconds. In the dilution module, the LNP precursor was mixed with citrate buffer through a larger microfluidic chip. The pH of solution was adjusted to nearly neutral and the ethanol concentration is reduced. The post-process module contained a SPTFF and a syringe filter. The SPTFF was designed for removal of ethanol and free RNA in the solution and concentrating of LNPs. The syringe filter was used to remove the bacteria in the solution. The modules were connected by

pipelines, constructing an enclosed environment to decrease the risk in containment of LNPs. Furthermore, an on-line monitoring system including optical system and AI visual recognition was developed to analyze the mixing of ethanol and water in microfluidic chips.

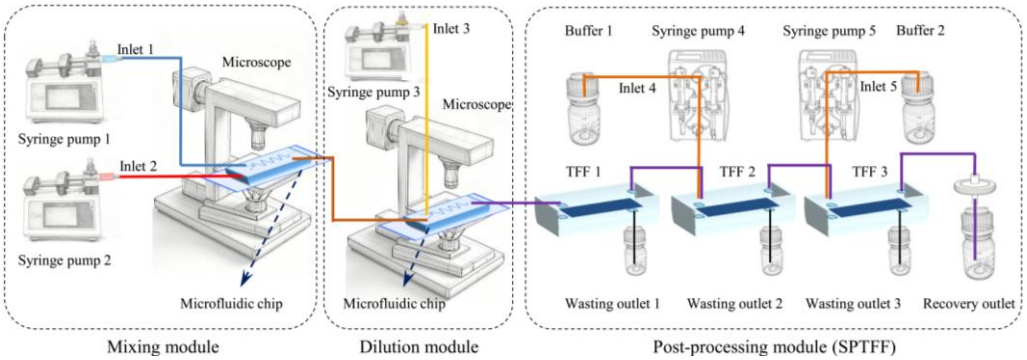

Figure 2 Schematic diagram of the full-flow microfluidic platform

2.1 Microfluidic chips

The microfluidic chips were fabricated based on soft lithography techniques. The silicon master molds for PDMS were purchased from *CapitalBio Technology*. Sylgard™ 184 PDMS kits were mixed by stirring with a ratio of 10:1 and PDMS mixture was subjected to vacuum degassing for 10min. The degassed PDMS mixture was poured onto the silicon master molds, which subsequently suffered from vacuum degassing and baking at 90 ℃ for 45 min. The cured PDMS was peeled off the master mold and the pre-designed recesses were formed in the cured PDMS. Eventually, the PDMS was irreversibly bonded to a glass slide through plasma treatment under 100 W and 50 Pa for 1 min. The bonding between the PDMS and the glass slide was enhanced through overnight incubation. As observed in Figure 3, the microfluidic chip in mixing module was designed with spiral channels to greatly decrease the dead zone, same to that in dilution module. The channels were provided with constant cross-section dimensions of 100 μm×100 μm along the channel paths, compared with that of 200 μm×200 μm for dilution module (4 times the retention volume).

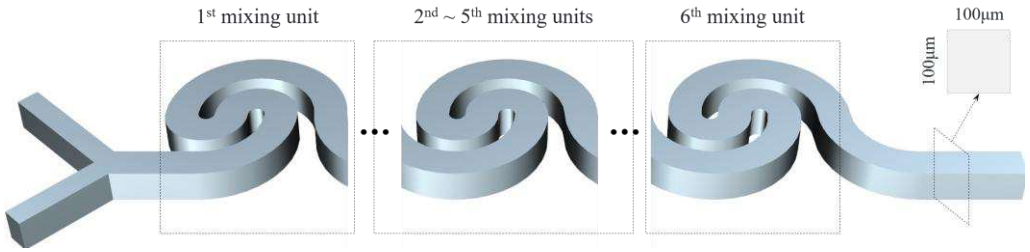

Figure 3. Detailed designs of the microfluidic chips in mixing module

2.2 SPTFF

During the synthesis of LNPs, small molecules like ethanol, unreacted lipids and free RNA were

removed through SPTFF. Different to the traditional TFF, circulation process was not needed, causing less effect of the high shear zone in pumps on the LNPs. The SPTFF was composed of three identical TFFs connected in series. The first two TFFs were designed to remove the free small molecules, and the third TFF was designed to concentrate the LNPs. Additional buffer could be supplied into each TFF and the expected solution could be collected from the recovery outlet. The TFF consisted of stainless steel clamp obtained by mechanical processing and PES membrane with a 100 kDa Molecular Weight Cut-Off. The seal between the stainless steel and the membrane was achieved using gaskets to prevent leakage under pressure. Figure 4 shows the flow process of the solution in single TFF module.

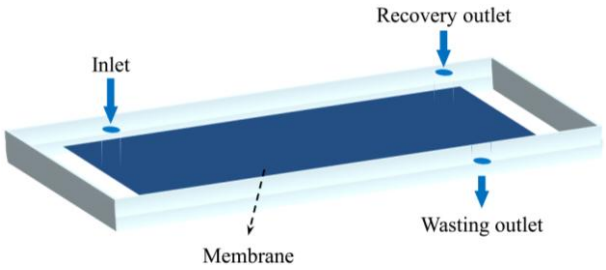

Figure 4 Schematic diagram of tangential flow filtrations (TFF)

2.3 Pumps and sensors

The ethanol with the dissolution of lipids and the water with the dissolution of RNA were respectively injected into the connected pipelines of the mixing module via two syringe pumps (Harvard, Pump 11). Another syringe pump (Oushisheng, HP-10) was used in the dilution module to supply additional citrate buffer, to decrease the concentration of ethanol and to adjust the pH of solution. Another two syringe pumps (Oushisheng, HP-10) were used to supply PBS buffer for SPTFF. Furthermore, the stability of the microfluidic platform was evaluated by microfluidic pressure senor and microfluidic flow rate senor (Elveflow, NFS).

2.4 AI-assisted monitoring system

The size and encapsulation of LNPs were significantly affected by the mixing of ethanol and water, difficult to realize the on-line monitoring through traditional methods. However, it was concluded that the mixing was changed with the illumination intensity of the image obtained under the bright field by microscope, as displayed in Figure 5. Therefore, an on-line monitoring system including optical system and AI visual recognition was developed to analyze the mixing of ethanol and water in microfluidic chip. The optical system was composed of a microscope (Hamamatsu ORCA-Fusion

sCMOS & Micro-Manager 2.0) and a computer (Dell). Firstly, 0.1% Rhodamine B was dissolved in ethanol for the mixing fluorescence and total flow rates were varied from 30 ml/h to 60 ml/h. The fluorescence intensity was measured through an inverted fluorescence microscope under excitation wavelength of 488 nm and the emission wavelength of 529 nm. A mixing index was used for mixing quantification based on fluorescence intensity, defined as followed. When the mixing index was greater than 0.9, the mixing label was set as "Good"; otherwise, the mixing label was "Bad".

$$M = 1 - \frac{\sqrt{\frac{1}{n}\sum_1^n (I_i - I_{ave})^2}}{\frac{\sum_1^n I_i}{n}} \quad (1)$$

where M and n denote mixing index and the total levels of intensity, respectively. I_i and I_{ave} refer to the ith fluorescence intensity and the average fluorescence intensity, respectively.

Meanwhile, the bright fields (without fluorescence) were measured under the same conditions as the above fluorescence measurements. A dataset could be obtained with bright field as input, mixing index and mixing label ("Good" or "Bad") as outputs, divided into a training dataset and a testing dataset for the AI model. As showed in Figure 6, the accuracy could reach to 97.3% in training dataset and 93.1% in testing dataset. During the following experiments of LNPs, the mixing index and mixing label could be directly given according to bright image from microscope, without the effect of trace molecules like I_2 or fluorescence dyes on LNPs.

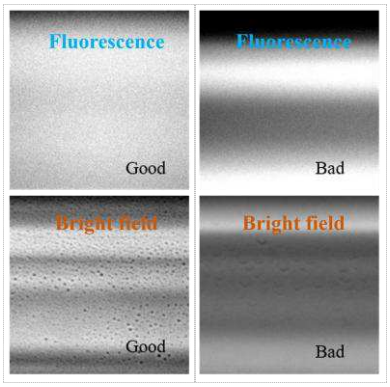

Figure 5 Observed images of mixing

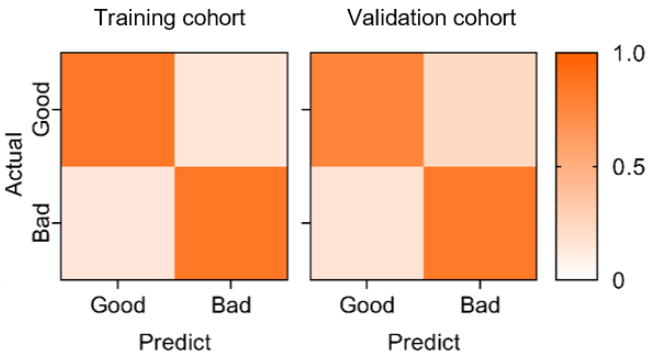

Figure 6 AI model to predict mixing label

3. Results and discussions

3.1 Experiments on mixing efficiency in microfluidic chips

Water and ethanol were injected into the mixing module under the flow rate ratio of 3:1. Firstly, the flow characteristics were numerically investigated with CFD (Computational Fluid Dynamics method, compared with the experimental results under the same condition. As shown in Figure 7,

the concentration field was provided with the similar distribution with fluorescence intensity, proving the feasibility of the present method. Besides, the secondary vortex flow on the cross section of the channel was clearly observed, considered as the main effect for mixing due to little turbulence in microchannel. The dead zone could be greatly decreased under the flow rate of 60 ml/h.

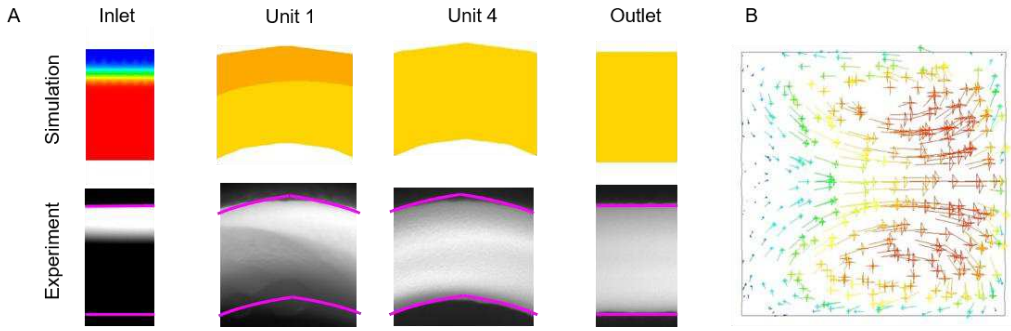

Figure 7 Mixing characteristics (A. concentration distraibution; B. flow vector)

Furthermore, the mixing in microfluidic chips were studied at various conditions. The detailed parameters were summarized in Table 1. According to the fluorescence intensity, the water and ethanol could be well mixed in the mixing module when the total flow rate was greater than 30 ml/h. As the total flow rate was increased to be above 50 ml/h, only 2~3 repeating mixing units resulted in ideal mixing between water and ethanol. But more repeating mixing units were needed for a complete mixing under lower flow rate. Therefore, higher flow rate enhanced better mixing, as achieved in 3.16 ms with 60 ml/h and 1.38 ms with 80 ml/h. The quantified mixing index was derived to give a threshold (M=0.9) of total flow rate for an ideal mixing, as shown in Figure 8.

Table 1 Experimental conditions on mixing in microfluidic chips

Chips	Inlets and outlets	Solvent	Flow rate/(ml/h)	Ratio
Microfluidic chip in mixing module	Inlet 1	Water	7.5~60	3
	Inlet 2	Ethanol	2.5~20	1
	Inlet 1+Inlet 2	25% ethanol-water solution	10~80	/
Microfluidic chip In dilution module	Inlet 1+Inlet 2	25% ethanol-water solution	20~80	1
	Inlet 3	water	80~320	4
	Inlet 1+Inlet 2+Inlet 3	5% ethanol-water solution	100~400	/

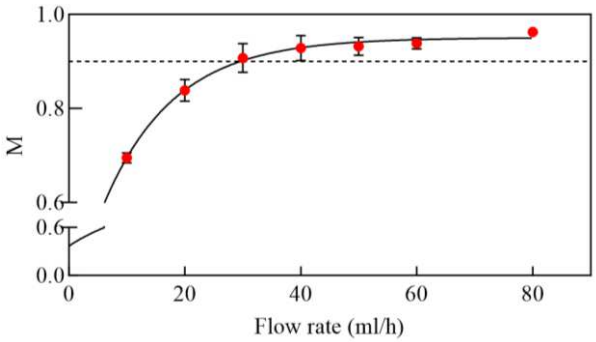

Figure 8 Relationship between mixing index and total flow rate

The microfluidic chip in the dilution module was design with 4 times the volume of the previous chip, to reduce ethanol concentration from 25% to 5% and to adjust pH of LNP solution to neutral. The experimental conditions were also listed in Table 1. As observed in Figure 9, the ethanol-water solution could be completely mixed with the buffer in the microfluidic chip, achieved within 10 ms. According to the mixing index of microfluidic chips in Figure 10, similar mixings could be achieved in the mixing module and dilution module, indicating little effect of microfluidic chips connected in series on the mixing. Therefore, the mixing and buffer exchange could be completed in 1min through a continuous flow solution, much more efficient than the traditional dialysis or ultrafiltration.

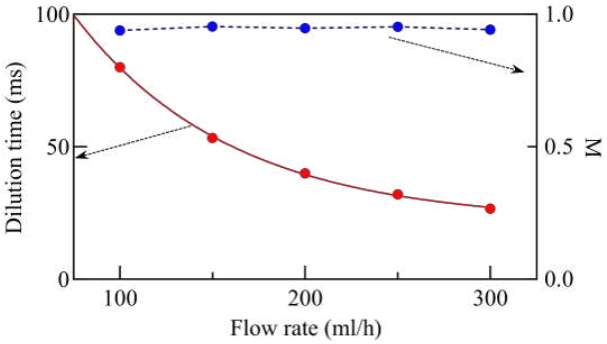

Figure 9 Mixing index and dilution time in dilution chip

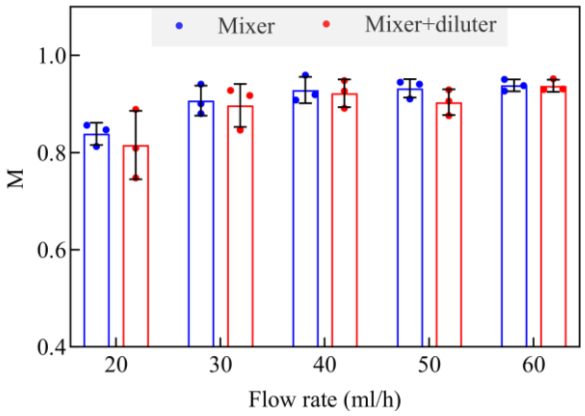

Figure 10 Similar mixing in microfluidic chips of mixing and dilution modules

3.2 **Experiments on filtration by SPTFF**

The performances of SPTFF contains macromolecule retention and small molecule removal. The first work was conducted with 100 nm fluorescence PS particles, similar in size to the present LNPs. The correlation between the fluorescence intensity and PS concentration (0.033%~1.0%) was obtained based on a microplate reader under the extension wavelength of 480 nm and emission wavelength of 510 nm, presented in Figure 11. Besides, PEG-20k, namely PEG with average molecular weight of 20,000 was selected to study the molecular removal of unreacted lipids (less than 3 kDa) and free siRNA (about 15 kDa). A linear relationship between the peak area measured by LC-RID and PEG-20k mass concentration was derived, as shown in Figure 12.

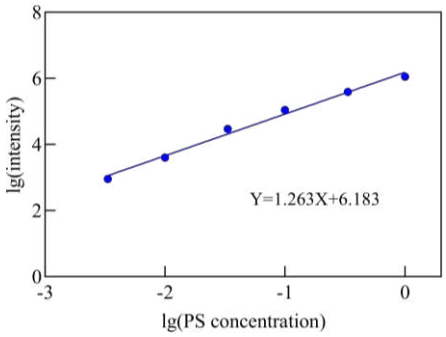

Figure 11 Correlation for PS concentration

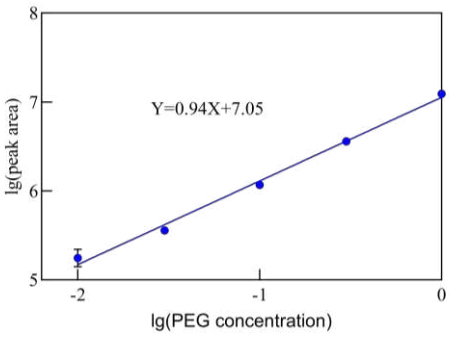

Figure 12 Correlation for PEG concentration

The PS solutions or PEG-20k solutions from three wasting outlets and recovery outlet were collected to measure the fluorescence intensity, peak area and volumes, respectively. The mass concentration of PS or PEG were extrapolated according to the correlations in Figure 11 and Figure 12. The recovery rate of PS or PEG was calculated by mass concentrations and volumes, derived by:

$$\mathrm{R} = \frac{C_4 \times V_4}{C_0 \times (\sum_1^4 V_i)} \tag{2}$$

where R represents recovery rate of PS particle. C and V refer to the concentration of PS particles and solution volume collected from the outlet, respectively. The subscript 0 is the inlet of SPTFF; i (=1~3) represents i^{th} wasting outlet; 4 is the recovery outlet.

100 kDa PES membranes were used in the three TFFs of SPTFF to separate the LNPs with small molecules. Due to the little pressure drop in the primary flow of SPTFF, the three TFFs were considered with the similar transmembrane pressures yielded by back pressures. Therefore, one TFF was used to individually study the flux performances in this section. In order to match the flow conditions for complete mixing in mixing and dilution modules, experiments with the upstream flow rate of 150~300 ml/h (equivalent to 30~60 ml/h in mixing module) were conducted for flux

performances under few risks to damage the microfluidic chips. The related parameters were listed in Table 2. The back pressure was varied to achieve 10%~100% solvent permeability.

Table 2 Experimental conditions on filtration performances of SPTFF

Aims	Inlet (TFF 1)				Inlet 4 (TFF 2)		Inlet 5 (TFF 3)		Recovery outlet
	Solvent	Simulated solute	Mass concentration	Flow rate /(ml/h)	Solvent	Flow rate /(ml/h)	Solvent	Flow rate /(ml/h)	Back pressure /(kPa)
Flux tests of TFF	Water	/	/	150	/	/	/	/	30~90
				200					25~130
				250					30~140
				300					40~180
Retention tests of macromolecule	Water	PS particles	0.1%	200	Water	170	Water	170	112
				200		180		180	117
				200		190		190	123
				250		213		213	120
				250		225		225	127
				250		238		238	133
Filtration tests of small molecules	Water	PEG-20k	0.8%	200	Water	170	Water	170	112
				200		180		180	117
				200		190		190	123
				250		213		213	120
				250		225		225	127
				250		238		238	133

It could be seen from Figure 13 that the solvent permeability increased linearly with the back pressure within the scope of the present conditions. Considering the removal efficiency of small molecules, a solvent permeability of 90% was used in the following study. When the upstream flow rates were 150 ml/h, 200 ml/h, 250 ml/h and 300 ml/h, the back pressures were changed to be about 80 kPa, 120 kPa, 130 kPa and 170 kPa, respectively. When the SPTFF was used in actual conditions, additional buffer was supplied to the next TFF due to the solvent permeability of the last TFF.

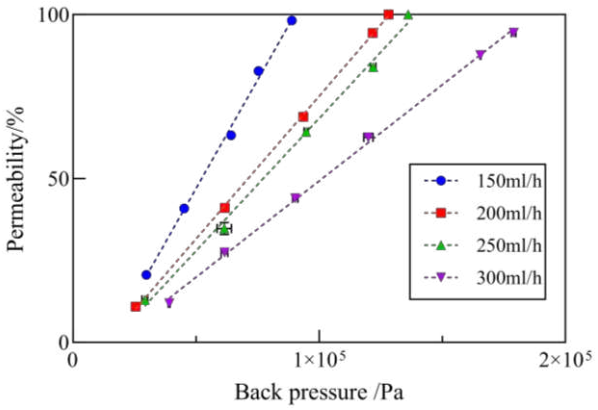

Figure 13 Flux performance of SPTFF under complete mixing

Figure 14 presented the flow process and experimental results under some available condition. The flow rate of upstream water into the first TFF was 250 ml/h and the followed two TFFs were supplied with a same water flow rate of 225 ml/h. The water volumes collected from three wasting outlets and one recovery outlet were measured to about 8.2 ml, 8.0 ml, 8.1 ml and 1.2 ml, respectively. The removal efficiency of the solvent and the concentration factor were calculated to be about 99.8% and about 7.59, respectively. It could be inferred that the water could flow smoothly through the TFFs in series and that the SPTFF could work very well with a designed permeability of 90%.

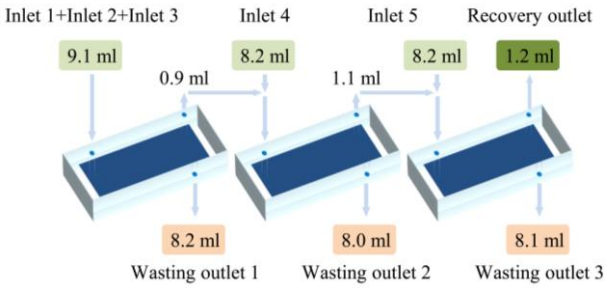

Figure 14 Schematic diagram of upstream flow and supplies in SPTFF

During the retention tests of macromolecule, the PS mass concentrations of solutions from outlets were calculated according to the linear correlation on log coordinates in Figure 11. The flow rates were consistent with the above condition. The initial mass concentration of PS particles was about 0.1%. The solution from the recovery outlet was measured to have a 0.79% mass concentration and the intensities of the solutions from three wasting outlets were found close to the background, indicating few PS particles to penetrate through the membranes. Combined with the solvent permeability of 89% measured in experiment, the calculated recovery rate was approximately 87%. Therefore, the SPTFF developed in the present study could undertake the recovery and concentration of particles with size greater than 100 nm.

Furthermore, the removal of small molecules in the SPTFF were validated using PEG-20k due to greater molecular weight than siRNA (about 15 kDa) and lipids (less than 3 kDa) used in the present study. And PEG, PEG lipid and DLin-MC3-DMA were linear molecules. If the PEG-20k could successfully permeate through the membrane, the unreacted lipids and free siRNA could be considered with the better removal by the SPTFF. The flow rates were consistent with the above optical condition. The PEG-20k concentration of upstream flow was about 0.8 mg/ml (~0.8%). A PEG-20k concentration of about 0.0127 mg/ml (~0.013%) was obtained from recovery outlet, only 1.6% of initial concentration of injected solution. The normalized concentrations were shown in

Figure 15. Approximately 90% of PEG-20k were filtered out in TFF 1. The solution concentration out of TFF 3 was higher than that of TFF 2, due to the concentrating of solution. Considering the concentration factor of 7.59 obtained above, 99.83% of the PEG-20k was removed, suggesting the removal performances of the SPTFF for unreacted lipids and free siRNA.

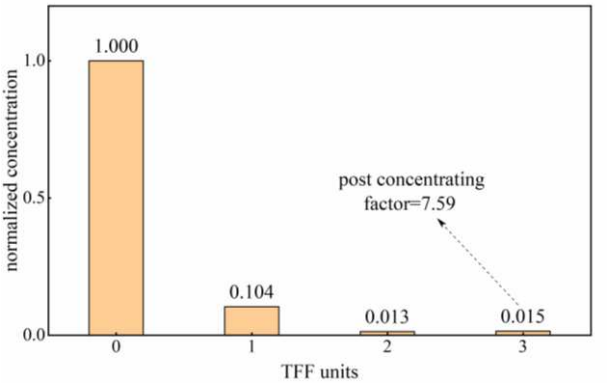

Figure 15 Normalized concentration of PEG-20k in SPTFF

3.3 **Experiments on siRNA encapsulation in LNPs**

Firstly, the standard correlation between siRNA concentration and fluorescence intensity was researched by a microplate reader (MOLECULAR, SpectraMax M2), which was given in Figure 16. The fluorescence intensity was analyzed with extension wavelength of 488 nm and emission wavelength of 550 nm. The solution with LNPs synthesized by the microfluidic platform was collected in centrifugation tubes and divided into two parts. The first part was piped into a 96-well plate, treated directly by NA-Green kit (*Beyotime biotechnology*). The average fluorescence intensity was measured in a plate reader, marked with I_{out}. The other part was firstly treated by 0.1% Triton X-100 for 30 min and subsequently by NA-Green kit. The average fluorescence intensity was recorded with I_{all}. The encapsulation efficiency was defined by:

$$\mathrm{E} = \frac{I_{all} - I_{out}}{I_{all}} \times 100\% \tag{3}$$

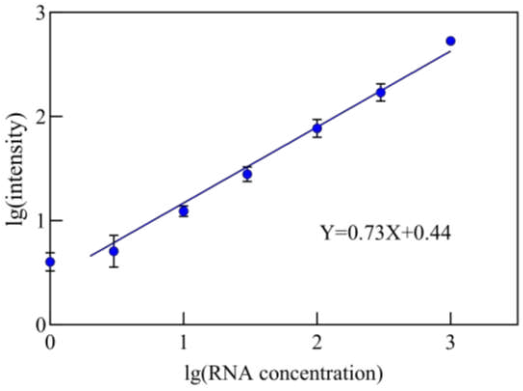

Figure 16 Correlation of fluorescence intensity with siRNA concentration

The evaluations of LNP encapsulation were performed with a FDA-approved LNP formulation of Onpattro® including Dlin-MC3-DMA, DSPC, cholesterol and PEG2000-DMG. The lipids solution was prepared by dissolving four lipids in ethanol at a molar ratio of 50:10:38.5:1.5. The patisiran siRNA (GUAACCAAGAGUAUUCCAUTT & TTCAUUGGUUCUCAUAAGGUA) was used to dissolve in the RNase free 10 mM citrate buffer, forming a solution at pH of 4.0. Table 3 presented the detailed flow conditions. The lipids solutions and the nucleic acid solutions were injected into the mixing module with the designed conditions listed in Table 3. Additional citrate buffer at pH of 8.0 was suppled into the dilution module with 4 times the flow rate of the mixed solution from the mixing module. Subsequently, the LNP solution flowed into the SPTFF, processed by PBS buffer. The synthesized LNPs were collected in centrifugation tubes. The size distributions and zeta-potentials of the LNPs were measured by DLS (Malvern) with dispersant of water, the RI of 1.45 and absorption of 0.001, respectively.

Table 3 Experimental conditions on encapsulation characteristics of LNPs

No.	Mixing module					Dilution module	SPTFF	
	Lipid solution into inlet 1 (lipids in ethanol)		Nucleic acid solution into inlet 2 (siRNA in citrate buffer)		Flow rate of mixed solution/(ml/h)	Flow rate of citrate buffer/(ml/h)	Flow rate of PBS buffer /(ml/h)	
	Concentration of lipids/(mg/ml)	Flow rate /(ml/h)	Concentration of siRNA/(ug/ml)	Flow rate /(ml/h)		Inlet 3	Inlet 4	Inlet 5
E-1	11.72	5.0	200	15.0	20	80	90	90
E-2	11.72	7.5	200	22.5	30	120	135	135
E-3	11.72	10.0	200	30.0	40	160	180	180
E-4	11.72	12.5	200	37.5	50	200	225	225
E-5	11.72	15.0	200	45.0	60	240	270	270
E-6	5.86	12.5	100	37.5	50	200	225	225
E-7	17.58	12.5	300	37.5	50	200	225	225
E-8	11.72	12.5	100	37.5	50	200	225	225
E-9	11.72	12.5	400	37.5	50	200	225	225

The pH values of the solutions were monitored at the outlets of the mixing module, the dilution module and the SPTFF, measured as 4.29, 6.80 and 7.25, respectively. Compared with the ionizable cationic lipid Dlin-MC3-DMA (pKa=6.44), this lipid existed in a cationic form within the mixing

chip, enabling electrostatic complexation with negatively charged siRNA. The solution pH after post-dilution exceeded the pKa of Dlin-MC3-DMA, indicating that the majority of the ionizable cationic lipid had transitioned to its neutral state. The effect of electronic repulsion was reduced and the LNP assembly was successfully completed. The pH changes in the chips of the mixing and dilution modules were designed to match with the pKa of lipid Dlin-MC3-DMA and the self-assembly of LNPs, reported in several literatures.

Firstly, the effect of the solution flow rate on the characteristics of LNPs was researched with the constant molar ratio of nitrogen in lipids to phosphorus in siRNA (N:P), as seen from E-1~E-5 in Table 3. The size distributions of LNPs at different flow rates were shown in Figure 17, which presented good agreements with some Gaussian distributions. The average size of LNPs decreased inversely with the flow rate, indicating better mixing to produce smaller LNPs. When the total flow rate of lipids solution and siRNA solution was 20 ml/h, the LNPs were provided with average size of 121.2 nm and PDI of 0.1483. When the total flow rate was increased to 60 ml/h, the average size and PDI were decreased to 83.49 nm and 0.1303, respectively. Therefore, LNPs could be precisely prepared with low PDI based on the present microfluidic platform, for tissue-specific delivery etc.

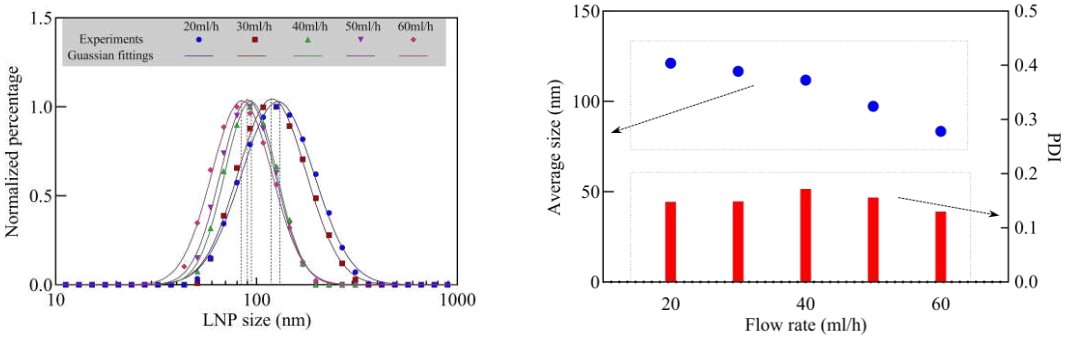

Figure 17 Effect of flow rate on LNPs' size (A. size distribution; B. Average size and PDI)

After the fluorescence intensity of the processed solution was measured, the siRNA concentrations were calculated according to the correlation in Figure 16. The encapsulation efficiency of LNPs could be obtained based on Equation 3. According to the results without purification of SPTFF, a positive correlation between encapsulation efficiency and flow rate was observed in Figure 17, when the flow rate was less than 50 ml/h. It was attributed to greater flow rate enhancing mixing and diffusion. But the encapsulation efficiency was little affected by further increased flow rate, indicating that optimal mixing was achieved in the present microfluidic chips under the flow rate of 50 ml/h. Additionally, the solution of LNPs from the dilution module was pumped into SPTFF to

remove the unreacted lipids and free siRNA. After the purification of SPTFF, the encapsulation efficiency of siRNA was approximately increased to above 96.7%. If more TFFs were connected in series, higher encapsulation efficiency could be achieved for purer LNPs.

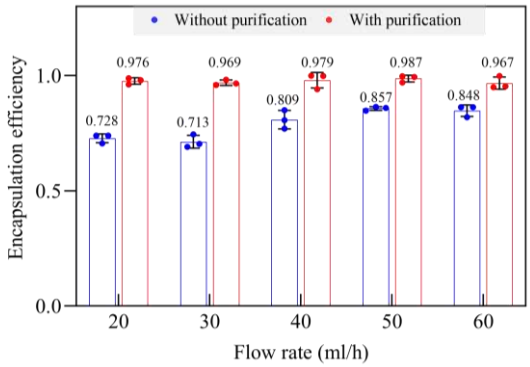

Figure 18 Encapsulation efficiency at different flow rates

Moreover, the concentrations of lipids and siRNA were simultaneously changed under the constant N:P of 10 and total flow rate of 50 ml/h. It could be found from Figure 19 that the size distributions also agreed well with some Gaussian functions. And the average size of LNPs increased with the concentration of siRNA (constant N:P), which might be caused by more fusion of primary micelles or intermediates and slighter diffusion at higher concentration of lipids. When the concentration of lipids was increased to17.85 mg/ml or more, aggregation and fusion were decreased by increased local viscosity, producing a little portion of small LNPs and a majority of large LNPs.

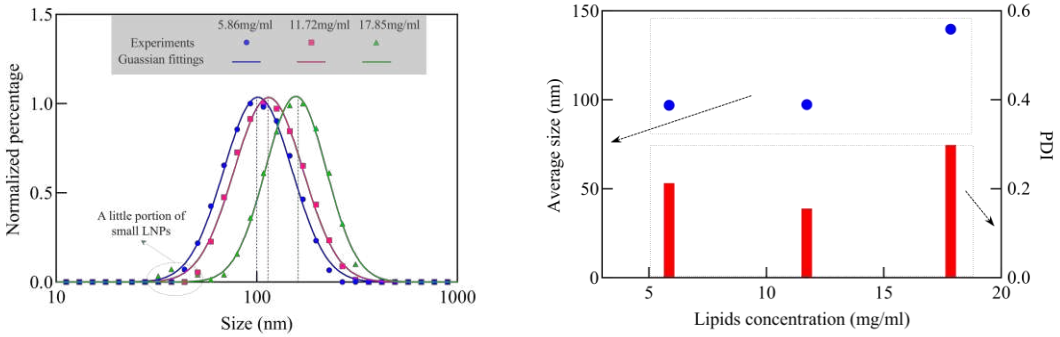

Figure 19 Effect of concentrations of lipids and siRNA on LNPs' size (A. size distributions; B. Average size and PDI)

Figure 20 presented the effect of the concentrations of lipids and siRNA on the encapsulation efficiency. According to the results without purification of SPTFF, the encapsulation efficiency was varied reversely with the lipids concentration. When the lipids concentration was increased to 17.85 mg/ml or more, aggregation and fusion were greatly affected by local viscosity, limiting the formation and encapsulation of LNPs. The encapsulation efficiency was decreased to 67.9%,

dramatically less than 85.7% at lipids concentration of 11.72 mg/ml. Because the mixing in microfluidic chips was mainly induced by laminar flow, the change of solution viscosity needs to be further considered on the mixing and mass transfer. Under low-concentration conditions, the encapsulation efficiency could be increased to 96.4% and 98.7% with purification of SPTFF. However, high lipids concentration resulted in more absorption of free siRNA on LNPs. After the purification of SPTFF, a majority of free siRNA was filtered and a small fraction of free siRNA remained absorbed on the LNPs. An encapsulation efficiency of 91.2% was calculated, significantly lower than those at low concentrations.

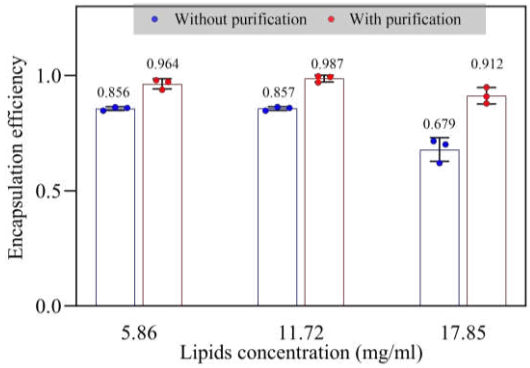

Figure 20 Encapsulation efficiency at different concentrations of lipids and siRNA

Finally, the concentration of siRNA was changed from 100 ug/ml to 400 ug/ml, to study the effect of N:P on size distribution and encapsulation efficiency under the constant total flow rate of 50 ml/h and lipids concentration of 11.72 mg/ml. Similar to the above results, the size distributions agreed well with some Gaussian functions, as seen in Figure 21. The average size of LNPs slightly increased with siRNA concentration, exhibiting an average size of about 100 nm.

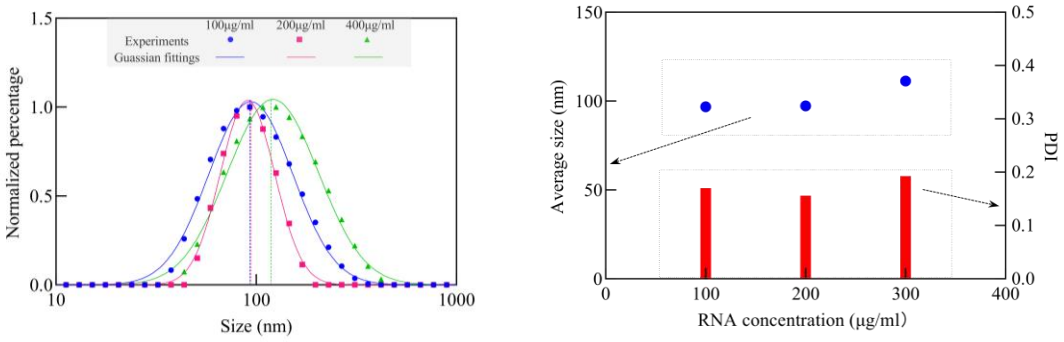

Figure 21 Effect of siRNA concentrations on LNPs' size (A. size distribution; B. Average size and PDI)

According to the reported studies, the encapsulation efficiency of LNPs was greatly affected by N:P. As shown in Figure 22, excess lipids could result in underutilization, yielding a low encapsulation

efficiency at low concentration of siRNA (high N:P). When the siRNA concentration was increased to an suitable N:P, electrostatic interactions between negatively charged siRNA and positively charged ionizable lipids were enhanced under acidic conditions, stimulating more siRNA encapsulated into LNPs (~86% at siRNA concentration of 100~400 ug/ml). If the siRNA concentration was further increased, excess siRNA could not be encapsulated by limited lipids, leading to a decrease in encapsulation efficiency. After the purification of SPTFF, the encapsulation efficiency could be increase to above 96% in the present conditions. Under the standard condition (E-4), an encapsulation efficiency of 98.7% could be obtained with SPTFF purification, meeting the requirement of >98% encapsulation efficiency for high-end formulations.

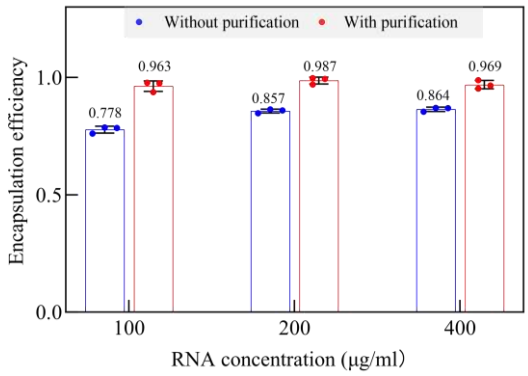

Figure 22 Encapsulation efficiency at different siRNA concentrations

4. Conclusions

In the present study, a full-flow microfluidic method was advanced for the synthesis and purification of LNPs. The end-to-end process referred to synthesis, purification and concentrations of LNPs without materials transfer and additional post processing. The mixing in microfluidic chips, the removal of small molecules and retention of macromolecule, and the characteristics of LNPs were investigated, respectively. Some conclusions were listed as followed.

(1) Despite the researchers' experience or lack thereof, the synthesis of LNPs could be completed in 15 min with little human interventions. Materials transfer and additional post processing were excluded in the present platform, greatly decreasing the risks in contaminations of LNPs. An AI model was proposed to examine the mixing efficiency without the effect of trace molecules on LNPs.

(2) The effect of flow rate, the concentrations of lipids and siRNA, and siRNA concentration (N:P changed from 20 to 5) on the characteristics of LNPs was further investigated based on the

microfluidic method. A positive correlation of mixing index with flow rate was analyzed, using for the selection of optimal flow conditions. The size distribution at different conditions agreed well with some Gaussian distributions. The average size of LNPs increased with lipids concentrations within some concentrations, but little affected by siRNA concentration.

(3) The average size and encapsulation efficiency of LNPs were sensitively influenced by mixing index, concentrations of lipids and siRNA, and siRNA concentration (N:P). High lipids concentration could result in great viscosity to impede the formation of LNPs and much absorption of free siRNA on LNPs difficult to purify. Therefore, the experimental optimization was crucial for optimal conditions including mixing, lipids concentrations and N:P. Under the present condition E-4, the encapsulation efficiency was approximately 85.7% without SPTFF purification and could be increased to 98.7% by the SPTFF processing, which could meet the requirement of >98% encapsulation efficiency for high-end formulations.

CRediT authorship contribution statement

Jian Tao: Conceptualization, Methodology, Investigation, Formal analysis, Data curation, Writing – original draft, Writing - review & editing; **Junxiang Zhao**: Conceptualization, Resources, Experiments, Data curation, Writing – original draft; **Yuanyuan Liu**: Experiments, Project management, Writing – original draft; **Liang Hu**: Resources, Methodology, Validation, Data curation, Writing – original draft, Formal analysis, Writing – review & editing, Project administration; **Hongru Zhou**: Writing – original draft; Resources, Data curation, Supervision; **Bohui Wang**: Platform setup; Experiments, Data curation; **Yong Kang**: Writing – review & editing, Formal analysis, Methodology, Supervision.

Declaration of competing interest

The authors declare that they have no known competing financial interests or personal relationships that could have appeared to influence the work reported in this paper.

Acknowledgements

The authors greatly appreciate Asymchem Life Science (Tianjin) Co., Ltd. to support this research

and Dr. Cheng Yi Chen for constructive guidance for the manuscript.

References

[1] Hou, X., Zaks, T., Langer, R., et al., 2021. Lipid nanoparticles for mRNA delivery. Nat Rev Mater 6, 1078-1094. https://doi.org/10.1038/s41578-021-00358-0.

[2] Kanasty, R., Dorkin, J.R., Vegas, A., et al., 2013. Delivery materials for siRNA therapeutics. Nature Materials 12, 967-977. https://doi.org/10.1038/nmat3765.

[3] Han, X., Zhang, H., Butowska, K., et al., 2021. An ionizable lipid toolbox for RNA delivery. Nat Commun 12, 7233. https://doi.org/10.1038/s41467-021-27493-0.

[4] Barbier, A.J., Jiang, A.Y., Zhang, P., et al., 2022. The clinical progress of mRNA vaccines and immunotherapies. Nat Biotechnol 40, 840-854. https://doi.org/10.1038/s41587-022-01294-2.

[5] Setten, R.L., Rossi, J.J., Han, S.-p., 2019. The current state and future directions of RNAi-based therapeutics. Nature Reviews Drug Discovery 18, 421-446. https://doi.org/10.1038/s41573-019-0017-4.

[6] Pardi, N., Hogan, M.J., Porter, F.W., et al., 2018a. mRNA vaccines - a new era in vaccinology. Nat Rev Drug Discov 17, 261-279. https://doi.org/10.1038/nrd.2017.243.

[7] Lindsay, K.E., Bhosle, S.M., Zurla, C., et al., 2019. Visualization of early events in mRNA vaccine delivery in non-human primates via PET–CT and near-infrared imaging. Nature Biomedical Engineering 3, 371-380. https://doi.org/10.1038/s41551-019-0378-3.

[8] Wei, T., Cheng, Q., Min, Y.L., et al., 2020. Systemic nanoparticle delivery of CRISPR-Cas9 ribonucleoproteins for effective tissue specific genome editing. Nat Commun 11, 3232. https://doi.org/10.1038/s41467-020-17029-3.

[9] Leppek, K., Byeon, G.W., Kladwang, W., et al., 2022. Combinatorial optimization of mRNA structure, stability, and translation for RNA-based therapeutics. Nat Commun 13, 1536 https://doi.org/10.1038/s41467-022-28776-w.

[10] Hu, B., Zhong, L., Weng, Y., et al., 2020. Therapeutic siRNA: state of the art. Signal Transduct Target Ther 5, 101. https://doi.org/10.1038/s41392-020-0207-x.

[11] Akinc, A., Maier, M.A., Manoharan, M., et al., 2019. The Onpattro story and the clinical translation of nanomedicines containing nucleic acid-based drugs. Nature Nanotechnology 14, 1084-1087. https://doi.org/10.1038/s41565-019-0591-y.

[12] Kristen, A.V., Senda, A.-D., Isabel, C., et al., 2019. Patisiran, an RNAi Therapeutic for the Treatment of Hereditary Transthyretin-Mediated Amyloidosis. Neurodegenerative Disease Management 9, 5-23. https://doi.org/10.1056/NEJMoa1716153.

[13] Polack, F.P., Thomas, S.J., Kitchin, N., et al., 2020. Safety and Efficacy of the BNT162b2 mRNA Covid-19 Vaccine. N Engl J Med 383, 2603-2615. https://doi.org/10.1056/NEJMoa2034577.

[14] Pardi, N., Parkhouse, K., Kirkpatrick, E., et al., 2018b. Nucleoside-modified mRNA immunization elicits influenza virus hemagglutinin stalk-specific antibodies. Nat Commun 9, 3361. https://doi.org/10.1038/s41467-018-05482-0.

[15] Li, B., Manan, R.S., Liang, S.Q., et al., 2023. Combinatorial design of nanoparticles for pulmonary mRNA delivery and genome editing. Nat Biotechnol 41, 1410-1415. https://doi.org/10.1038/s41587-023-01679-x.

[16] Phua, K.K.L., Nair, S.K., Leong, K.W., 2014. Messenger RNA (mRNA) nanoparticle tumour vaccination. Nanoscale 6, 7715-7729. https://doi.org/10.1039/C4NR01346H.

[17] Rojas, L.A., Sethna, Z., Soares, K.C., et al., 2023. Personalized RNA neoantigen vaccines stimulate T cells in pancreatic cancer. Nature 618, 144-150. https://doi.org/10.1038/s41586-023-06063-y.

[18] Wang, X., Liu, S., Sun, Y., et al., 2023. Preparation of selective organ-targeting (SORT) lipid nanoparticles (LNPs) using multiple technical methods for tissue-specific mRNA delivery. Nature Protocols 18, 265-291. https://doi.org/10.1038/s41596-022-00755-x.

[19] Bian, X., Guo, Q., Yau, L.F., et al., 2025. Berberine-inspired ionizable lipid for self-structure stabilization and brain targeting delivery of nucleic acid therapeutics. Nat Commun 16, 2368. https://doi.org/10.1038/s41467-025-57488-0.

[20] Belliveau, N.M., Huft, J., Lin, P.J., et al., 2012. Microfluidic Synthesis of Highly Potent Limit-size Lipid Nanoparticles for In Vivo Delivery of siRNA. Mol Ther Nucleic Acids 1, e37. https://doi.org/10.1038/mtna.2012.28.

[21] He, Z., Hu, Y., Nie, T., et al., 2018. Size-controlled lipid nanoparticle production using turbulent mixing to enhance oral DNA delivery. Acta Biomater 81, 195-207. https://doi.org/10.1016/j.actbio.2018.09.047.

[22] Kim, J., Eygeris, Y., Gupta, M., et al., 2021. Self-assembled mRNA vaccines. Adv Drug Deliv Rev 170, 83-112. https://doi.org/10.1016/j.addr.2020.12.014.

[23] Heyes, J., Palmer, L., Bremner, K., et al., 2005. Cationic lipid saturation influences intracellular delivery of encapsulated nucleic acids. Journal of Controlled Release 107, 276-287. https://doi.org/10.1016/j.jconrel.2005.06.014.

[24] Kulkarni, J.A., Darjuan, M.M., Mercer, J.E., et al., 2018. On the Formation and Morphology of Lipid Nanoparticles Containing Ionizable Cationic Lipids and siRNA. ACS Nano 12, 4787-4795. https://doi.org/10.1021/acsnano.8b01516.

[25] Kulkarni, J.A., Witzigmann, D., Leung, J., et al., 2019. Fusion-dependent formation of lipid nanoparticles containing macromolecular payloads. Nanoscale 11, 9023-9031. https://doi.org/10.1039/C9NR02004G.

[26] Kulkarni, J.A., Witzigmann, D., Leung, J., et al., 2019. On the role of helper lipids in lipid nanoparticle formulations of siRNA. Nanoscale 11, 21733-21739. https://doi.org/10.1039/C9NR09347H.

[27] Chen, D., Love, K.T., Chen, Y., et al., 2012. Rapid Discovery of Potent siRNA-Containing Lipid Nanoparticles Enabled by Controlled Microfluidic Formulation. Journal of the American Chemical Society 134, 6948-6951. https://doi.org/10.1021/ja301621z.

[28] Liu, C., Feng, Q., Sun, J., 2019. Lipid Nanovesicles by Microfluidics: Manipulation, Synthesis, and Drug Delivery. Adv Mater 31, e1804788. https://doi.org/10.1002/adma.201804788.

[29] Kimura, N., Maeki, M., Sato, Y., et al., 2018. Development of the iLiNP Device: Fine Tuning the Lipid Nanoparticle Size within 10 nm for Drug Delivery. ACS Omega 3, 5044-5051. https://doi.org/10.1021/acsomega.8b00341.

[30] Mihaila, R., Chang, S., Wei, A.T., et al., 2011. Lipid nanoparticle purification by Spin Centrifugation–Dialysis (SCD): A facile and high-throughput approach for small scale preparation of siRNA–lipid complexes. International Journal of Pharmaceutics 420, 118-121. https://doi.org/10.1016/j.ijpharm.2011.08.017.

[31] Sakurai, Y., Tomoya, H., Harashima, H., 2017. Scalable preparation of poly(ethylene glycol)-grafted siRNA-loaded lipid nanoparticles using a commercially available fluidic device and tangential flow filtration. Journal of Biomaterials Science, Polymer Edition 28, 1086-1096. https://doi.org/10.1080/09205063.2017.1291297.

[32] Bolze, H., Riewe, J., Bunjes, H., et al., 2021. Protective Filtration for Microfluidic Nanoparticle Precipitation for Pharmaceutical Applications. Chemical Engineering & Technology 44, 457-464.

https://doi.org/10.1002/ceat.202000475.

[33] Chen, X., Chen, H., Wu, D., et al., 2018. 3D printed microfluidic chip for multiple anticancer drug combinations. Sensors and Actuators B: Chemical 276, 507-516. https://doi.org/10.1016/j.snb.2018.08.121.